Sensors and Actuators B 239 (2017) 923–932

Contents lists available at ScienceDirect

Sensors and Actuators B: Chemical

journal homepage: www.elsevier.com/locate/snb

H_2O_2 sensing enhancement by mutual integration of single walled carbon nanohorns with metal oxide catalysts: The CeO_2 case

María Victoria Bracamonte[a,b], Michele Melchionna[a], Angela Giuliani[a], Lucía Nasi[c], Claudio Tavagnacco[a], Maurizio Prato[a,d,e,*], Paolo Fornasiero[a,f,*]

[a] Department of Chemical and Pharmaceutical Sciences, INSTM. University of Trieste, Via L. Giorgieri 1, 34127 Trieste, Italy
[b] FaMAF, Universidad Nacional de Córdoba, IFEG, Conicet,Ciudad Universitaria, M. Allende s/n, 5000 Córdoba, Argentina
[c] CNR-IMEM Institute, Parco Area delle Scienze 37/A, 43124 Parma, Italy
[d] Carbon Nanobiotechnology Laboratory, CIC biomaGUNE, Paseo de Miramón 182, 20009 Donostia-San Sebastian, Spain
[e] BasqueFdnSci, Ikerbasque, Bilbao 48013, Spain
[f] ICCOM-CNR, University of Trieste, via Giorgieri 1, 34127 Trieste, Italy

ARTICLE INFO

Article history:
Received 20 July 2016
Received in revised form 16 August 2016
Accepted 19 August 2016
Available online 20 August 2016

Keywords:
Carbon nanohorns
Cerium dioxide
Hydrogen peroxide
Electro-catalysis
Sensor

ABSTRACT

The importance of sensing hydrogen peroxide (H_2O_2) is due to its ubiquity, being extensively used in industry and also being a biologically relevant side-product of several enzymatic processes. Electrochemical sensing is one of the most robust and simple methods for sensing H_2O_2 and the discovery of new electroactive materials, particularly at the nanoscale, represents a very hot topic of research. Here, we prove that upon appropriate integration of oxidized single-walled carbon nanohorns (ox-SWCNHs) into a *per se* moderate H_2O_2 sensor such as cerium dioxide (CeO_2), the sensitivity toward H_2O_2 is enhanced by almost two orders of magnitude (from 0.4 to 160 $\mu A\,cm^{-2}\,mM^{-1}$), on par with that of state-of-the-art metal or metal oxide-based sensors. The modified electrode is also very stable (82% response after 2 weeks of continuous use) and the results highly reproducible. The developed nanohybrid ox-SWCNHs@CeO_2, characterized fully and whose average size is about 70 nm as measured by both TEM and AFM, was also tested in real case studies such as washing liquids and milk and was confirmed to be a robust and highly selective material, being not affected neither by the presence of complex matrices, nor by interferents in several organic substrates. The high recovery confirmed the excellent specificity and flexibility of this new electrocatalytic material.

1. Introduction

Hydrogen peroxide (H_2O_2) is produced annually in 2.2×10^6 tons worldwide and is a ubiquitous compound, mainly used as strong oxidant, bleaching agent in the paper and textile industries and as a component or a reagent in detergents [1–3]. Moreover, in bio-organisms, H_2O_2 is an important side product of several enzymes and functions as a signalling molecule to regulate various bio-processes, such as immune cell activation, apoptosis, stomatal closure and root growth [4]. H_2O_2 is also worldwide sold as an antiseptic at concentrations of 3–10% wt in H_2O. The European Commission database for information on cosmetic substances and ingredients (CosIng) delimited the acceptable concentration of peroxide in cosmetic products between 0.1 and 12% wt depending on the particular end product (i.e. hair-care, skin-care, nail-hardening or oral hygiene) [5]. Hence, simple and sensitive detection of H_2O_2 in commercial samples has a high practical significance from a number of perspectives [3]. Some methods based on titration, fluorescence [6], chemiluminescence [7] and spectrophotometry [8] have been employed for H_2O_2 determination, with variable linear ranges of H_2O_2 concentration (from 10^{-2} to 10^{-10} M), and detection limits that have been reported to be as low as 10^{-11} M [9]. Nevertheless, each of these methods suffers from important drawbacks. For instance, the most common reactants for titration ($KMnO_4$ and $CeSO_4$) can oxidize the organic matter present in the sample matrix, leading to an overestimation of the H_2O_2 concentration. On the other hand, spectrophotometric methods often exhibit incompatibility with samples containing dispersed particulate or dissolved species which can absorb light in a broad wavelength range. Among the various available analytical techniques, electrochemical methods provide a rapid, sensitive, and cost effective

* Corresponding authors at: Department of Chemical and Pharmaceutical Sciences, INSTM. University of Trieste, Via L. Giorgieri 1, 34127 Trieste, Italy.
E-mail addresses: prato@units.it (M. Prato), pfornasiero@units.it (P. Fornasiero).

http://dx.doi.org/10.1016/j.snb.2016.08.112
0925-4005/

methodology [10]. Metal electrode materials, such as platinum and gold or glassy carbon electrodes have been proposed as sensors, but they are not devoid of disadvantages, such as high overpotentials (0.6 V and −0.1 V vs Ag/AgCl for oxidation and reduction of H_2O_2, respectively), slow kinetic and irreversible poisoning [11]. Noble metal-based nanoparticles certainly represent a definite advance, although negatively associated to high cost and low availability of the precious metal [12], as well as a tendency to aggregate during operation, thus diminishing their activity. These aspects highlight the necessity of modifying the electrode with alternative materials with improved catalytic performances, able to efficiently accelerate the H_2O_2 oxidation or reduction rates lowering also the required overpotentials. In this respect, a powerful approach, which can be considered as a state-of-the-art model, relies on electrochemical techniques based on enzyme-modified electrodes [13]. Enzymes such as horseradish peroxidase (HRP), catalase, cytochrome c, hemoglobin, microperoxidase and myoglobin [9] have been successfully employed and exhibited excellent sensitivity. From a practical point of view, however, the use of enzyme-modified electrodes is hampered by costly enzyme purification protocols [14], limited lifetime due to the denaturation of the enzyme [15], inherent instability, and complicated immobilization procedures [16]. For this reason, replacement of enzymes with all inorganic-based electrodes for hydrogen peroxide sensing represents a very attractive alternative. A new emerging concept holding great promise is the development of non-enzymatic H_2O_2 sensors based on hybrid nanomaterials, which feature high sensitivity, simple immobilization protocols and improved stability. Modern trends are moving toward the utilization of cheaper and more available metals or metal oxides, combined at the nanoscale level in hybrid inorganic-organic materials. In particular, the combination with nanostructured carbon materials such as carbon nanotubes (CNTs) or graphene (G) is setting new frontiers in many fields, including sensors [17,18]. This is due to their outstanding set of properties and the synergistic effect arising when appropriately combined with inorganic phases [19]. In this context, single-walled carbon nanohorns (SWCNHs) have gained in very recent years an exponential surge of interest, in particular for electrocatalytic applications [20], and they are expected to soon replace the more classic CNTs for a variety of applications. Such high expectations evolve from the SWCNHs fascinating structure, which results in unprecedented properties and reactivity. SWCNHs in their pristine state present a high surface area of approximately 300 $m^2\,g^{-1}$ [21]. Moreover, this value can be significantly increased to 1006–1464 $m^2\,g^{-1}$, together with its pore volume (0.47–1.05 $mL\,g^{-1}$) upon oxidizing treatments [22], which remove the tips of the SWCNHs making the internal space available [23]. In addition, SWCNHs display high electric conductivity, ability to accumulate analyte, alleviation of surface fouling, capability to undergo surface functionalization with a gradient of reactivity (tips vs sidewalls) and electrocatalytic activity [24]. SWCNHs have also been used as electrolyte [25,26] as a substitute for $TiCl_4$, [27] and as a counter electrode in dye-sensitized solar cells [28,29]. Recent studies have shown that SWCNHs can electrocatalyze both the oxidation and reduction of H_2O_2 [30]. It is envisioned that engineering of electroactive materials for H_2O_2 detection through synthetic protocols that suitably merge their properties with those of SWCNHs may lead to considerable increase of sensing ability. This concept is proved here, where an inorganic moderate catalyst for H_2O_2 electroreduction is combined with ox-SWCNHs, resulting in a boost of performance. From the perspective of the inorganic component, largely available and robust metal oxides represent the most appealing choice, as confirmed by the increasing recent efforts in developing metal oxide-based electrocatalysts [31]. Over recent years, cerium dioxide (ceria, CeO_2) has emerged as a leading catalytic material for its free radical scavenging properties, which make it attractive for multiple applications in biology, medicine, environmental and energy related topics [32,33]. The many useful catalytic properties of ceria have been attributed to the presence of highly mobile lattice oxygen which facilitates the interconversion Ce^{3+}/Ce^{4+} [34]. H_2O_2 has a great affinity for ceria, and it is used for etching the surface of preformed nanoparticles [35] or as templating agent during hydrothermal synthesis [36]. The use of ceria as component in H_2O_2 sensors is well documented, particularly in combination with enzymes. Recently, Ujjain et al. [10] reported the use of fructose or hexamethylene-tetra-amine stabilized CeO_2 nanoparticles for the development of a simple and inexpensive enzyme-free H_2O_2 sensor in cell cultures to remedy the oxidation processes caused by H_2O_2. The proposed non-enzymatic sensor exhibits a maximum sensitivity of 21.13 $\mu A\,cm^{-2}\,mM^{-1}$ around one order of magnitude lower than those reported for state-of-the-art metal/metal oxide based sensors, such as Au–MnO_2 (101.6 $\mu A\,cm^{-2}\,mM^{-1}$) [37], Pt–MnO_2 (122.99 $\mu A\,cm^{-2}\,mM^{-1}$) [38] and Fe_2O_3 (181 $\mu A\,cm^{-2}\,mM^{-1}$) [39]. We selected CeO_2 as the catalytically active phase for our case study. The CeO_2 was downsized to the nanoscale with simultaneous improvement of its catalytically relevant electronic characteristics, by a well-suited interface of CeO_2 with ox-SWCNHs, through an optimized sol-gel method that allows a uniform covering and intimate contact of the two phases. This approach has the advantage to make most of the oxide shell available for an efficient interaction with H_2O_2 and therefore to allow a sustainable use of rather small ceria loadings (below 20 wt%). In particular, the resulting hybrid material becomes a very efficient electrocatalyst for the electroreduction of H_2O_2, with an enhancement of almost two orders of magnitude (from 0.4 to 160 $\mu A\,cm^{-2}\,mM^{-1}$) of the sensitivity, setting the stage for a revolutionary strategy to considerably improve the performances of existing metal oxide based H_2O_2 sensors. The ox-SWCNHs@CeO_2-modified electrode also exhibits high reproducibility, robustness and selectivity, able to detect H_2O_2 in complex matrices such as those of milk and cleaning liquid, while retaining a very good sensitivity after two weeks of continuous use. Moreover, such features are combined with a very easy protocol for the assembly of the working electrode. We believe that the effective performance is related to the electronic interaction between the two phases, with the SWCNHs scaffold allowing a more favourable electron transfer onto the ceria with consequent formation of Ce^{3+} ions, responsible for the H_2O_2 reduction. The present work highlights a very promising path for the establishment of a new cost-effective family of H_2O_2 sensors, borne from an engineered integration of SWCNHs into metal oxides.

2. Materials and methods

2.1. Chemicals and reagents

Potassium ferricyanide was purchased from Fluka. Ascorbic acid (AA) was purchased from Merck. Urea was provided from Baker. Hydroquinone, acetaminophen (AP), alpha-D-Glucose, Nafion® 117 solution, cerium(IV) tetrakis(decyloxide) and hydrogen peroxide (H_2O_2, 30%) were purchased from Sigma Aldrich. The phosphate salts (NaH_2PO_4 and Na_2HPO_4) were purchased from Carlo Erba. Single-walled carbon nanohorns (SWCNHs) were provided by Carbonium S.R.L. All reagents were of analytical grade and used without further purification. All solutions were prepared with ultra-pure water, purified by a Millipore System (18.2 MΩ cm).

For the real sample analysis Italian UHT Milk (3.5% of fat content) and a commercial clean liquid for clothes containing alcohol, dimethyl adipate, dimethyl glutarate, dimethyl succinate, C12-14 pareth-X, MEK, Poly(oxy-1,2-ethanediyl), alpha-isotridecyl-omega-hydroxy, alcohols, C16-18 and C18 unsaturedethoxylated and water, were used.

2.2. Apparatus and measurements

Thermogravimetric analyses (TGA) of approximately 1 mg of each compound was recorded on a TGA Q500 (TA Instruments) under air, by equilibrating at 100 °C, and following a ramp of 10 °C min^{-1} up to 800 °C. Raman spectra were recorded with an Invia Renishaw microspectrometer (50) equipped with He–Ne laser at 532 nm. To avoid sample damage or laser-induced heating/crystallization of the materials, the incident power was kept at 1%. Powders were dispersed in EtOH, drop-cast onto a quartz slide and the solvent evaporated; at least 5 spectra per sample were recorded on different areas of the sample in order to check the uniformity of the materials. Fourier Transform Infrared Spectroscopy (FTIR) was measured in a System 2000–Perkin Elmer spectrometer in an optical range of 370–4000 cm^{-1} at a resolution of 4 cm^{-1}. Transmission Electron Microscopy (TEM) measurements were performed on a TEM Philips EM208, using an acceleration voltage of 100 kV. Samples were prepared by drop casting from the dispersion onto a TEM grid (200 mesh, copper, carbon only). High resolution TEM (HRTEM) were acquired on a JEOL 2200FS microscope operating at 200 kV, equipped with an Energy Dispersive Spectrometer (EDX), in-column energy (Omega) filter, and High-Angle Annular Dark-Field (HAADF) detector. Atomic Force Microscopy (AFM) measurements were performed using a Nanoscope V microscope (Digital Instruments Metrology Group, model MMAFMLN) in tapping mode in air at room temperature, using standard μmasch® SPM probe (HQ:NSC15/AIBS) with tip height 12–18 μm, cone anglen <40° (Resonant frequency 325 kHz, force constant of ~40 N m^{-1}). Image analysis has been performed with Gwiddion software. N_2 physisorption at the liquid nitrogen temperature was collected using a Micromeritics ASAP 2020 analyzer. Before analysis, the samples were degassed at 150 °C for at least 12 h at a pressure lower than 10 mHg. The specific surface area of the samples was calculated applying the BET method. Pore size distributions were calculated applying the BJH method to the adsorption branch of the isotherms.

All electrochemical measurements were performed on a Autolab 302 N electrochemical workstation (Metrohm, The Netherlands) at room temperature, using a conventional three-electrode system composed of a modified glassy carbon electrode (GCE; CH Instrument, CH 104) as a working electrode, a platinum wire as an auxiliary electrode and a Ag/AgCl (3 M NaCl) (CH Instrument, CH 111) as a reference electrode. TRIS buffer (0.1 M, pH 7.4) was employed as the supporting electrolyte solution for the electrochemical experiments. The buffer solution was purged with high purity nitrogen for 15 min prior to experiments and left under the same gas atmosphere during the measurements. Amperometric experiments were conducted in a stirred TRIS buffer solution by applying the desired working potential and allowing the transient currents to decay to a steady-state value prior to the addition of the analyte.

EIS experiments were performed in the frequency range between 100,000 to 0.01 Hz, with a potential perturbation of 0.01 V and a working potential of −0.20 V using 25.0×10^{-3} M hydrogen peroxide. All presented results are averaged upon three independent measurements.

2.3. Synthesis of oxidized SWCNHs

Pristine single-walled carbon nanohorns (SWCNHs) were dissolved in a 4 M nitric acid solution in order to get a suspension 1.0 mg mL^{-1}. The suspensions were sonicated for 15 min to dissolve the present bundles and then stirred for three hours. Such time is the optimum to obtain a sufficient degree of oxygenic groups with low damage on the honeycomb structure surface. The solid was then filtered and washed with distilled water until neutral pH of the washing water.

2.4. Preparation of the ox-SWCNHs@CeO_2

The ox-SWCNHs@CeO_2 structures were prepared by a sol-gel method. The appropriate amount of the Ce^{4+} tetrakis(decyloxide) was dissolved in 25 mL of Tetrahydrofuran (THF). The solution was then transferred to a sonicator and a THF/*N*,*N*-Dimethylformamide (DMF) dispersion of ox-SWCNHs was added. The mixture was kept under sonication for 30 min. A mixture of H_2O (1 mL) and THF (10 mL) was added to ensure the complete hydrolysis of the alkoxide precursor, and the mixture was sonicated for an additional 15 min. The solids were then recovered by filtration and washed with THF three times. The final materials were then dried at 120 °C overnight prior to being used.

2.5. Electrode modification

Glassy carbon electrode was first polished with sand paper and then with 1.0 μm and 0.3 μm alumina powders (micropolish Buehler). After rinsing thoroughly with deionized water, it was sonicated in deionized water to remove any alumina residues, and was then cycled 3 times in 0.10 M phosphate buffer solution (PBS) between 0.9 and −0.3 V at 0.10 V s^{-1} to perform the electrochemical polishing. The surface state reproducibility was controlled for each electrode measuring one cyclic voltammogram in 1 mM potassium ferricyanide. Electrodes presenting a difference between redox peak potentials higher than 0.08 V were discarded. After the electrochemical polishing, the electrodes were allowed to dry in a stream of nitrogen. 10 μL of the ink-like suspension of corresponding materials (ox-SWCNHs, ox-SWCNHs@CeO_2) were then casted on the surface of clean GCE and dried in the oven at 50 °C for 30 min. Such prepared modified electrodes were defined as ox-SWCNHs/GCE and ox-SWCNHs@CeO_2/GCE, respectively.

The nanohorns' inks were prepared at a concentration of 2.5 mg mL^{-1} using Nafion® 1% in ethanolic:water (50:50) medium and treated in an ultrasonic bath for 30 min.

3. Results and discussion

3.1. Synthesis

The assembly of the final hybrid was achieved through a sol-gel method, combining mildly oxidized SWCNHs (ox-SWCNHs) with the precursor $Ce(ODe)_4$ (ODe = decyloxide) under sonication prior to hydrolysis. The mild oxidation of SWCNHs with diluted HNO_3 has the double function of equipping the carbon scaffold with COOH groups for anchoring the Ce precursor and of enhancing the surface area by tips removal of the carbon scaffold.

3.2. Characterization

Two distinct weight losses are observed in the TGA profile of ox-SWCNHs@CeO_2, Fig. 1.

The peak at ~200 °C is ascribed to the removal of water or combustion of the organic residues of the Ce precursor (decanol) and the oxy-groups on the SWCNHs surface. The second weight loss at temperatures between 300 and 400 °C is assigned to the combustion of the carbon nanostructure. Such a combustion temperature for the ox-SWCNHs component is considerably lower than that of free ox-SWCNHs, indicating that the carbon scaffold is in tight contact with CeO_2, thus fully exploiting its well-known oxidation ability, resulting in lowering of the combustion temperature [40]. The TGA profile of ox-SWCNHs confirms the absence of inorganic impurities in the material. From the TGA profile, we can also note that the

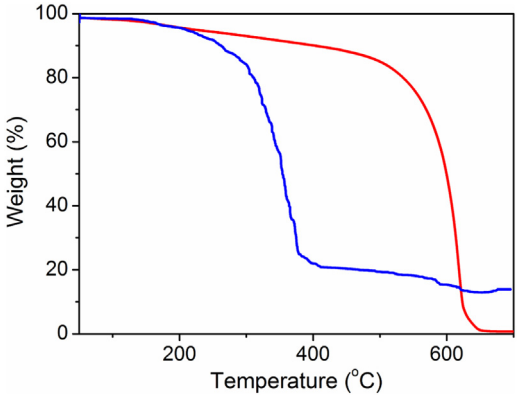

Fig. 1. TGA plots of the ( ) ox-SWCNHs and ( ) ox-SWCNHs@CeO_2 in air.

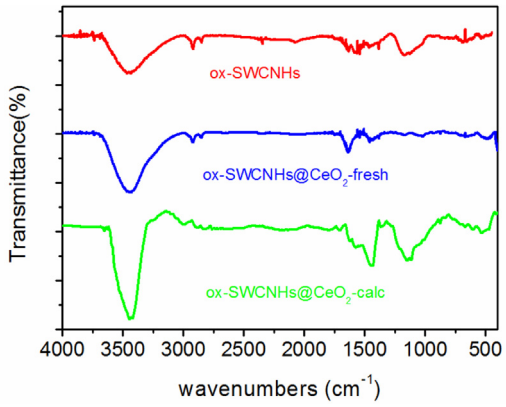

Fig. 2. FT-IR spectra of ( ) ox-SWCNHs, ( ) ox-SWCNHs@CeO_2 and ( ) calcined ox-SWCNHs@CeO_2.

CeO_2 content amounts to ~18% wt. The presence of hydroxylated CeO_2 is also confirmed by FTIR, Fig. 2.

The broad band at 3450 cm^{-1} corresponds to the O—H stretching of adsorbed water molecules. A small band at 494 cm^{-1} is present in the ox-SWCNHs@CeO_2 spectrum attributed to the Ce-O stretching [41], indicating the formation of CeO_2 around the nanostructure. The band observed at 1637 cm^{-1} can be ascribed to O—H bending of adsorbed water as well as to C=O stretching of the as-oxidized SWCNHs. The successful mild oxidation of the SWCNHs is also supported by the small band at 1170 cm^{-1}, attributed to the C—O stretching [7]. Interestingly, upon a thermal treatment of the sample at 250 °C, the band at 1637 cm^{-1} almost disappears, possibly confirming the removal of carboxylic acid functionalities from the SWCNHs surface or the removal of adsorbed water, while a more intense band is visible at ~1100 cm^{-1}. This latter band could be due to the creation of new C—O—C bonding [42] with the ceria oxygen atoms, which ensue the tight contact between the carbon and ceria phases after thermal treatment. Moreover, the Ce—O stretching band becomes more intense. Overall, the thermal treatment reduces the number of polar groups and increases the contact CeO_2-SWCNHs, and this could have an impact in disfavouring the adsorption of polar H_2O_2 molecules.

The analysis of the structures by Raman spectroscopy is presented in Fig. 3.

The spectrum shows the typical D and G bands pattern for nanocarbons: the D band at ~1330 cm^{-1}, the G band at ~1580 cm^{-1} and the 2D band ~2665 cm^{-1} [43]. The I_D/I_G ratio (~1.27) is not significantly affected with respect to the free ox-SWCNHs material indicating a minimal perturbation of the carbon scaffold properties by the addition of the metal oxide. No peaks associated to the CeO_2 modes are observed in the Raman spectra of ox-SWCNHs@CeO_2 due to its amorphous phase. However, irradiation with higher Raman laser powers (>5 mW) induces local crystallization, producing the appearance of the F_{2g} Raman peak characteristic of CeO_2 at 461 cm^{-1} (Fig. 3B) [44].

The intimate contact between the CNHs scaffold and the CeO_2, and the uniform covering, are confirmed by Scanning Transmission Electron Microscopy with a High-Angle Annular Dark-Field detector (HAADF-STEM) and Energy-Dispersive X-ray spectroscopy (EDX) (Fig. 4). Almost a perfect co-location of ox-SWCNHs and CeO_2 is observed. No isolated aggregates of CeO_2 were found upon thorough analysis of the sample. As expected, calcination induces a crystallization of the CeO_2 shell, as confirmed by High Resolution TEM (HRTEM) and Fast Fourier Transform (FFT) analysis of the material (Fig. S1).

Atomic Force Microscopy (AFM) confirms that upon drop casting of the material suspension onto a solid support, the nanohybrids disperse very uniformly, Fig. 5.

As can be seen on the several height profiles, single ox-SWCNHs@CeO_2 of very similar sizes (in the range 50–80 nm) are repeatedly observed, together with only minor aggregates. This has important consequences on the homogeneous covering and the improved efficiency of the catalyst-modified electrode. Thus, the as-prepared nanomaterial dispersions are suitable candidates for more advanced electrode surface modification techniques able to generate single layers of catalyst, thus maximising efficiency.

The electrochemical characterization of ox-SWCNHs@CeO_2 was carried out by first modifying a glassy carbon electrodes (GCE) with a nanohybrid ink dispersion by drop casting and measuring their response by Cyclic Voltammetry (CV) experiments in N_2-saturated 0.10 M TRIS-HCl buffer solution pH 7.4, with a scan rate of 0.10 V s^{-1}. Fig. 6 shows the obtained response. For the GCE and ox-SWCNHs/GCE no faradaic signal is observed, confirming the inertness of these materials within the explored potential window, while the redox signatures arising at −0.02 V and −0.14 V for ox-SWCNHs@CeO_2/GCE can be readily ascribed to Ce^{4+}/Ce^{3+} sites of the metal-oxide shell [7,45].

3.3. *Electrocatalytic response toward H_2O_2 by ox-SWCNHs@CeO_2 modified glassy carbon electrodes*

The electrocatalytic response toward H_2O_2 was first evaluated by cyclic voltammetry (CV). Since the detection of hydrogen peroxide at neutral pH is the most relevant and challenging case [11], the experiments were performed in N_2-saturated TRIS-HCl buffer solution at pH 7.4 in absence and presence of 5.00×10^{-3} M H_2O_2. Initially, the response of a bare CeO_2-modified glassy carbon electrode, using CeO_2 prepared by the same method used for the synthesis of the nanohybrid but in absence of ox-SWCNHs, was evaluated. No obvious current for H_2O_2 reduction was observed in the case of CeO_2/GCE indicating the poor electron transfer occurring at the oxide/GCE interphase (Fig. 7A). An appreciable increase in the cathodic current for the H_2O_2 reduction was observed in the presence of ox-SWCNHs (Fig. 7B) with an onset potential of −0.24 V (vs Ag/AgCl) with respect to that of the bare CeO_2 electrode. This response can be ascribed to the reduction of hydrogen peroxide by the carbon nanostructures [46]. When CeO_2 was incorporated to form the nanohybrid material, a remarkable enhancement in the faradaic response for H_2O_2 was noticed (Fig. 7C). In particular, the catalytic response increased in terms of current with a characteristic onset potential of −0.11 V.

The comparison of the faradic currents of the bare CeO_2, ox-SWCNHs and ox-SWCNHs@CeO_2 at −0.30 V, clearly indicates that the formation of the nanohybrid produces a remarkable enhancement of the current density with respect to the individ-

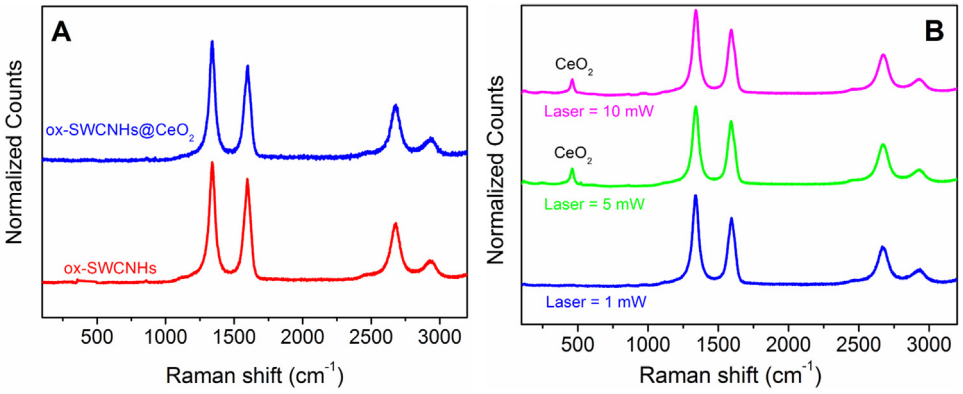

Fig. 3. A) Raman spectra of the ( ) ox-SWCNHs and ( ) ox-SWCNHs@CeO_2. B) Raman spectrum of ox-SWCNHs@CeO_2 at different laser powers 1, 5 and 10 mW.

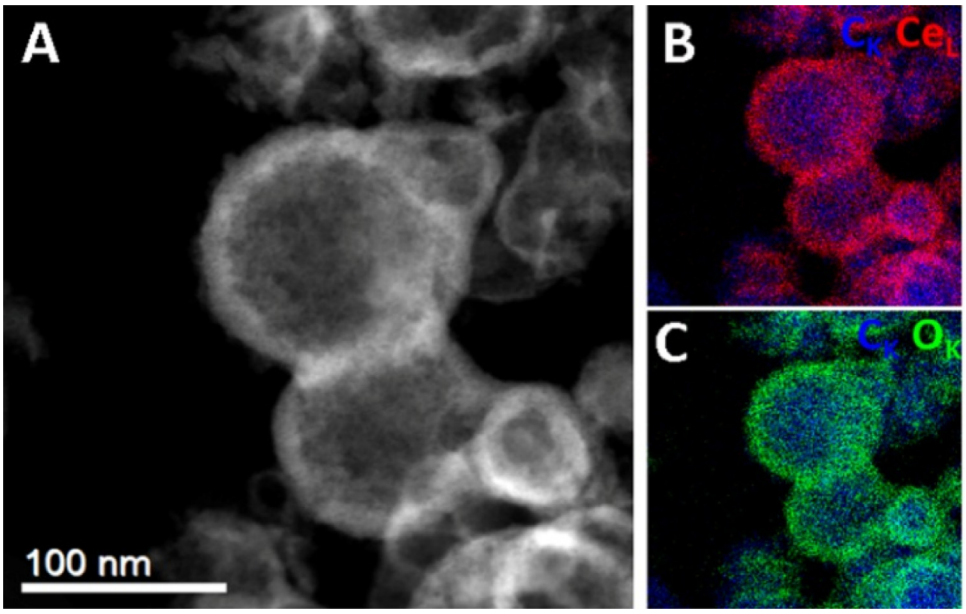

Fig. 4. A) Representative HAADF-STEM of ox-SWCNHs@CeO_2; B) EDX mapping of C and Ce atoms; C) EDX mapping of C and O atoms.

ual components CeO_2 and ox-SWCNHs, highlighting the synergy of the two phases in the electrocatalytic reduction of H_2O_2. The boost of the catalytic activity on ox-SWCNHs@CeO_2 can be attributed to i) the fast transition between Ce^{3+} and Ce^{4+}, changing the amount of oxygen vacancies in the CeO_2 and forming n-type hybrids [47] and ii) their synergistic combination with the nanocarbon component which increments the active area and reduces the energy barrier for the electron transfer. The electronic communication between the two phases, achieved with a highly successful synthetic protocol, is therefore an essential feature of the modified electrode, and can be used as a powerful strategy to improve the electronic characteristics of the metal oxide at the electrode interface.

For better understanding the electrochemical behaviour of GCE modified with ox-SWCNHs@CeO_2, Electrochemical Impedance Spectroscopy (EIS) was performed. Fig. 8 shows the Nyquist plots obtained in 2.50×10^{-2} M H_2O_2 at −0.20 V for ox-SWCNHs/GCE and ox-SWCNHs@CeO_2/GCE. The equivalent circuit used to fit the ox-SWCNHs/GC electrode's impedimetric response is (R_s($R_{ct}C_{dl}$)) where the solution resistance (R_s) is in series with the charge transfer resistance (R_{ct}) which is in parallel with the constant phase element that represents the double layer capacitance (C_{dl}). When the GCE is modified with ox-SWCNHs@CeO_2, the equivalent circuit includes two additional elements: a second capacitance (C_{II}) and a charge transfer resistance (R_{ct}II) associated with the electrocatalytic activity of the CeO_2 sites. When CeO_2 is incorporated, the charge transfer resistance decreases from $922 \pm 3\ \Omega\ cm^2$ to $188 \pm 4\ \Omega\ cm^2$ (R_{tc} and $R_{tc} + R_{tc}$II, respectively). In other words, the presence of CeO_2 in conjugation with the ox-SWCNHs favours the catalytic activity of the hybrid material towards hydrogen peroxide reduction by facilitating the charge transfer between the redox probe and the electrode surface.

The analytical performance of the three modified electrode (CeO_2, ox-SWCNHs and ox-SWCNHs@CeO_2) for the electrochemical reduction of H_2O_2 was also evaluated amperometrically. Fig. 9A shows the current-time recordings obtained at −0.20 V for successive additions of 20 μL of a 5.00×10^{-2} M H_2O_2 solution (corresponding to 1.0×10^{-4} M H_2O_2 final concentration) using an ox-SWCNHs@CeO_2 modified GC electrode. The corresponding calibration plot, as well as the calibration plots of the bare CeO_2 and ox-SWCNHs are depicted in Fig. 9B. For all materials a linear relationship between the density current and hydrogen peroxide concentration is obtained in the studied concentration range. Due to the poor electron transfer occurring at the oxide surface, the bare CeO_2 material exhibits a very low, although detectable, aver-

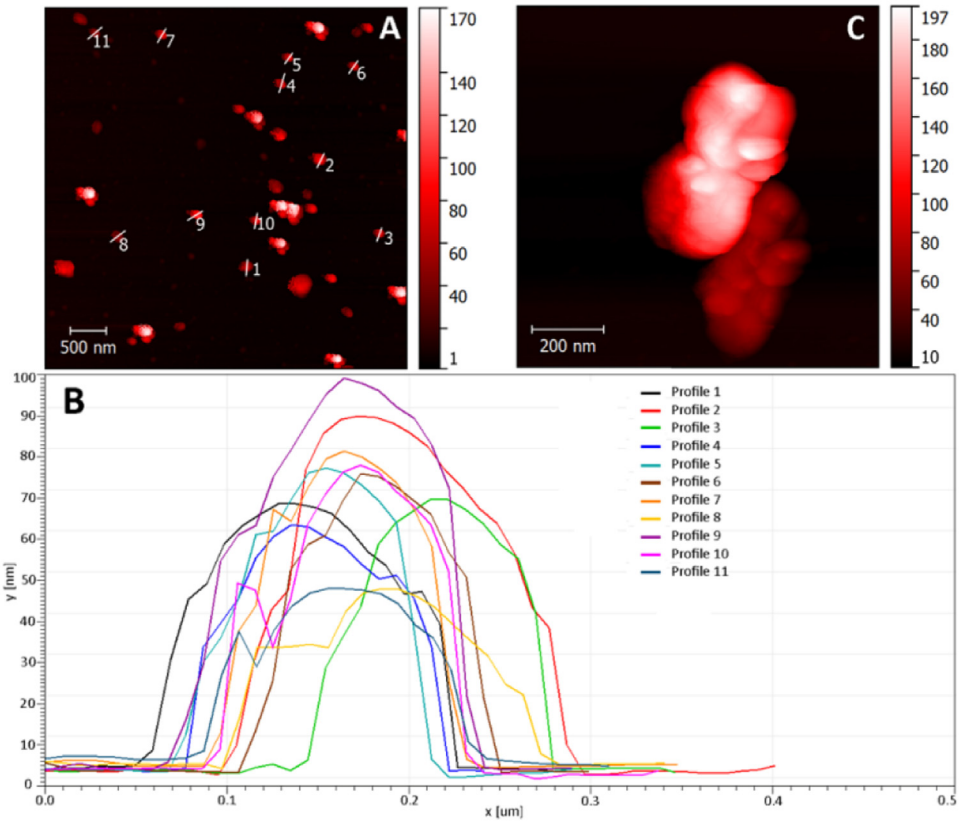

Fig. 5. A) Representative AFM image of a typical window of the drop casted sample. B) Corresponding heights profile measured on 11 particles (indicated in A). C) AFM expansion of a typical small aggregate where single SWCNHs@CeO_2 can be recognized.

age sensitivity of $0.4 \pm 0.1\ \mu A\ cm^{-2}\ mM^{-1}$ measured at −0.20 V. It is worth noting that the sensitivity is considerably lower than that of the other "only ceria" modified electrode for H_2O_2 sensing reported by Ujjain, where protected ceria nanoparticles exhibited a sensitivity of $\sim 20\ \mu A\ cm^{-2}\ mM^{-1}$ [10]. However, in the latter case, the loading of ceria was much higher and the material was also optimized from a synthetic point of view, with a formation of well-defined CeO_2 nanoparticles and the presence of protecting groups, that avoid aggregation. This difference in sensitivity is also an indication of the intrinsic benefits of confining the metal oxide to the nanoscale level. The average sensitivities measured at −0.20 V for the other two modified electrodes were $20 \pm 3\ \mu A\ cm^{-2}\ mM^{-1}$ and $160 \pm 20\ \mu A\ cm^{-2}\ mM^{-1}$ for ox-SWCNHs/GCE and ox-SWCNHs@CeO_2/GCE, respectively. It is interesting to note a moderate sensitivity for the electrode modified with ox-SWCNHs alone, which exceeds that of other reported systems based on metal oxides (Table S1). Most likely this arises from the improved electron transfer at the interface with the conductive nanodomains and highlights the promising use of ox-SWCNHs as component in H_2O_2 electrochemical sensors. Finally, the remarkably higher sensitivity of the nanohybrid ox-SWCNHs@CeO_2 confirms the synergy between the both materials, CeO_2 and ox-SWCNHs, and the critical maximization of the contact between the two phases, as previously concluded by CV and EIS experiments.

The stability over time of the electrode modified with ox-SWCNHs@CeO_2/GCE was analyzed by measuring the sensitivity of calibrations plots obtained from amperometric experiments at −0.20 V in the course of 14 days. As far as the stability is concerned, it is generally very variable across the systems developed for H_2O_2 detection. Based on literature data, we can rank the stability of our system as very good in comparison with sensors using metal oxides [48,58], with a 82% sensitivity retained after two weeks of continuous use (Fig. S3). The drop of performance is considerable after the first electrocatalytic cycle, mostly because of the detachment, during operation, of the loosely anchored part of the material from the electrode. The performance then gradually decreases in the next days probably due to additional small leaching of the material from the electrode. However, the obtained stability highlights the great potential held by the material.

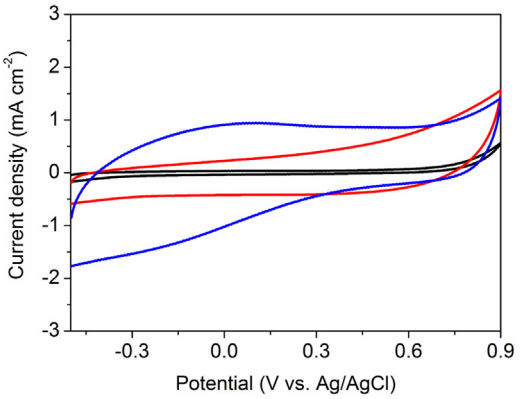

Fig. 6. CVs obtained on bare ( ) and modified GCE with ox-SWCNHs ( ) and ox-SWCNHs@CeO_2 ( ) in 0.10 M TRIS-HCl buffer solution pH 7.40 under N_2. Scan rate: $0.10\ V\ s^{-1}$ between −0.50 V and 0.90 V vs Ag/AgCl.

Another important aspect in the development of a hydrogen peroxide sensor is the evaluation of the interference of easily oxidizable compounds present in commercial samples such as ascorbic acid, glucose and paracetamol. Fig. 10 displays ampero-

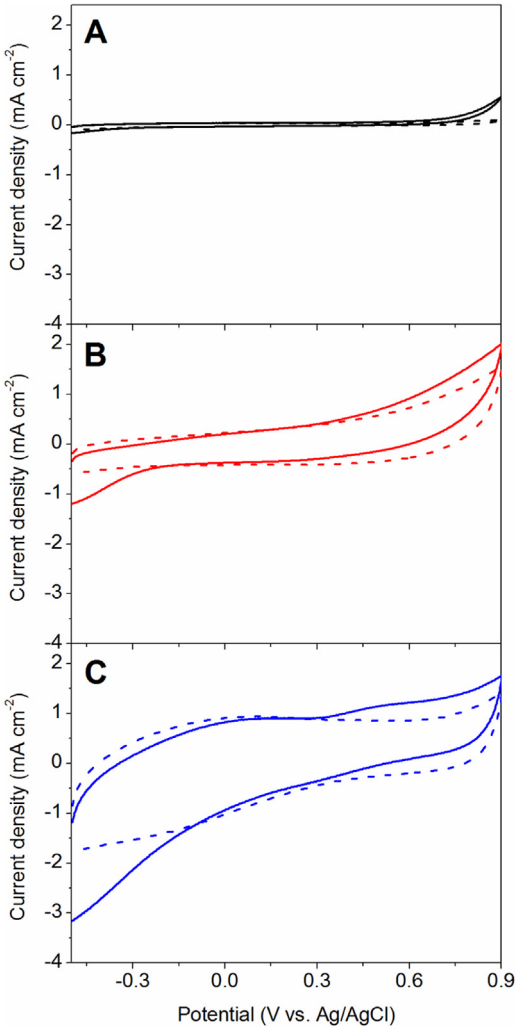

Fig. 7. CVs at GCE modified with bare CeO_2 (A), ox-SWCNHs (B) and ox-SWCNHs@CeO_2 (C) in 0.10 M Tris-HCl buffer solution without (dash line) and with (solid line) 5.00×10^{-3} M H_2O_2. Scan rate: 0.10 V s^{-1}.

metric recordings at −0.20 V obtained after addition of H_2O_2 in order to reach a final concentration of 2.00×10^{-4} M, followed by the same additions of ascorbic acid, glucose and acetaminophen.

While there is a definite sudden drop of current upon addition of H_2O_2, there is no obvious current response observed with the addition of these interfering substances, demonstrating the high selectivity of the sensor.

3.4. Effect of thermal treatment of CeO_2 on the electrochemical response

In order to further understand the mechanism and considering that the electrochemical performances of ceria based materials are strongly dependent on its structure (particle size, morphology and Ce^{3+}/Ce^{4+} content), the samples were thermally treated to lead to crystallization of the CeO_2. Therefore, the effect of calcination of ox-SWCNHs@CeO_2 samples, at 250 °C for 5 h, on the electrochemical performance was investigated. Fig. 11 shows comparatively the sensitivity of the fresh and calcined sample.

An important decrease in the sensitivity is observed after the calcination of the materials, with values dropping to ~55 ± 30 μA cm^{-2} mM^{-1}. Consistently, Chen et al. reported that the concentration of O—Ce^{3+} and of the hydroxyl groups decreased at calcination temperatures higher than 400 °C [49]. In addition, taking into account the results of Karakoti et al. [50] on the peroxide's decomposition catalyzed by CeO_2 (Eqs. (1) and (2)):

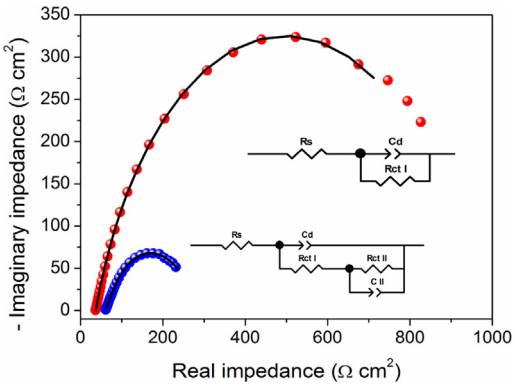

Fig. 8. Nyquist plots obtained for ox-SWCNHs/GCE ( ) and ox-SWCNHs@CeO_2/GCE ( ). Points indicate the experimental data, lines the corresponding fit with the equivalent circuits presented as an inset.

Table 1
Summary of the textural properties of the investigated materials.

Sample	Specific Surface Area[a] (m^2/g)	CPV[b] (mL/g)	D_{max}[c] (nm)
Ox-SWCNHs@CeO_2-fresh	212	1.002	98
Ox-SWCNHs@CeO_2-calc	570	1.008	100

[a] Calculated from BET analysis.
[b] CPV = Cumulative pore volume.
[c] Relative maxima of the pore size distributions obtained by the BJH analysis of the adsorption branch of the isotherms.

$$Ce^{4+} + H_2O_2 \rightarrow Ce^{3+} + HOO^{\bullet} + H^+ \quad (1)$$

$$Ce^{4+} + HOO^{\bullet} \rightarrow Ce^{3+} + O_2 + H^+ \quad (2)$$

We can relate the decrease in sensitivity to the increment in the Ce^{4+} content after the calcination, which favours the decomposition of the hydrogen peroxide prior to its electrochemical reduction. We also investigated whether the change in sensitivity may be at least partially ascribed to a variation of the textural properties of the material following calcination. To this purpose, N_2 physisorption isotherms were recorded at liquid nitrogen temperature over the fresh and calcined. Both materials exhibit Type IV isotherms according to IUPAC recommendations [51], with such type being typical of mesoporous materials (Fig. S4). The pore diameter ranges around 100 nm (Fig. S5), a value that does not significantly change with the thermal treatment, and the cumulative pore volume is high (Table 1). However, the surface area considerably increases after the calcination, passing from 212 to 570 m^2 g^{-1}. This is expected as the calcination removes all the organics, and clearly indicates that the difference in sensitivity cannot be attributed to a decrease of surface area or change of pore volume.

On the other hand, such decrease in activity might be related to the removal of polar functionalities (COOH and OH groups on SWCNHs and, more importantly, of part of the OH groups on CeO_2) from the surface of the material caused by the thermal treatment, as also indicated by FTIR analysis (see above) which therefore disfavours adsorption of polar H_2O_2 molecules.

3.5. Detection of H_2O_2 in relevant commercial case studies

Selectivity, matrix effects and interference are the common problems of application of sensors in real samples analysis. With the aim to study these effects, we investigated the applicability of the hybrid ox-SWCNHs@CeO_2 system for detecting H_2O_2 in a

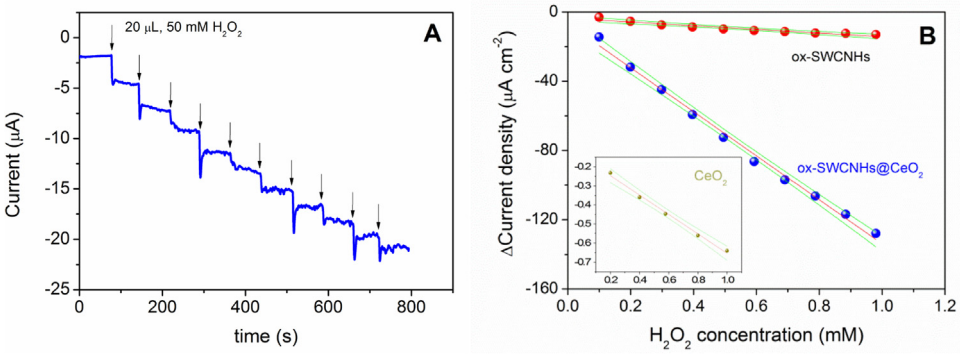

Fig. 9. A) Amperometric plot for additions of 5.00×10^{-2} M H_2O_2 solution using ox-SWCNHs@CeO_2/GCE. Arrows indicate the addition. B) Calibration plots obtained from the amperometric response presented in A with ox-SWCNHs@CeO_2 (●) and from ox-SWCNHs/GCE (●). For clarity, the inset present the calibration plot (on a different current density scale) obtained with CeO_2/GCE. (▬) are the linear fit to the data and (▬) indicate the 95% confidence bands.

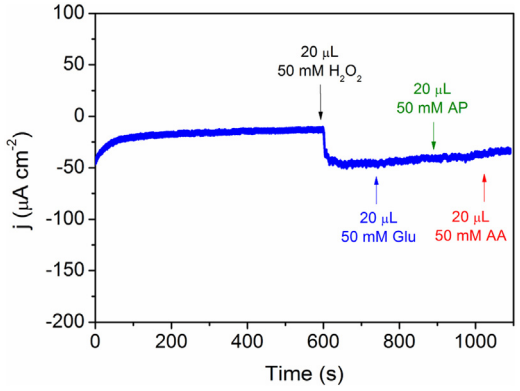

Fig. 10. Current-time profile at ox-SWCNHs@CeO_2/GCE for one addition of H_2O_2 in order to reach a final concentration of 2.00×10^{-4} M, followed by the same additions of ascorbic acid (AA), glucose (Glu) and acetaminophen (AP).

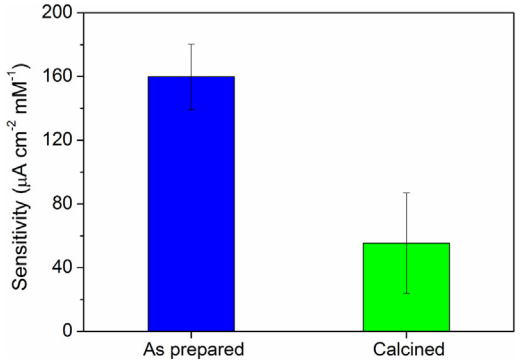

Fig. 11. Sensitivity to H_2O_2 obtained from amperometric experiment at −0.20 V using glassy carbon electrodes modified with calcined and fresh ox-SWCNHs@CeO_2 dispersions.

milk sample and a cleaning liquid, where the co-presence of many additive may render very problematic H_2O_2 accurate sensing.

Hydrogen peroxide is widely used as a preservative in milk and milk products because of its potential to inhibit microbial proliferation and milk spoilage. In United States [52], Brazil [53] and others countries, the addition of H_2O_2 to milk is not allowed, with the exception of certain applications prior to cheese-making and during the preparation of modified whey. However, due to the matrix interference on the H_2O_2 detection, building a specific and highly performing sensor is not an easy task. Thus, samples made of commercial Italian UHT milk (3.5% fat content) as matrix were assayed in order to demonstrate the application of the nanohybrid based sensor to commercial products.

In the experimental setup, 10 μL of milk were diluted in 10 mL of 0.1 M TRIS-HCl (pH 7.4). Subsequently, known amounts of H_2O_2 were added, and their recoveries were determined using amperometric measurements. The analysis shows a recovery percentage of 110% with 8% of relative standard deviation (RSD).

To further probe the applicability of the sensor in real samples, its electrochemical response to H_2O_2 was also verified in commercial cleaning liquid, where H_2O_2 is often added as bleaching agent and disinfectant. However, H_2O_2 tends to rapidly decompose to water and oxygen, decreasing the quality of the product. For this reason, quality checks are conducted by detecting the concentration of H_2O_2. A method to determine the peroxide content in this category of products is made challenging by the co-presence of various and complex organic molecules, such as dimethyl adipate, dimethyl glutarate, dimethyl succinate, C12-14 Pareth-X, MEK, poly(oxy-1,2-ethanediyl), alpha-isotridecyl-omega-hydroxy, C16-18 alcohols and C18 unsaturated alcohol which can interfere with the analysis. In the current experiment, the cleaning liquid sample was diluted 625 times with a 0.1 M TRIS-HCl (pH 7.4) and known amounts of H_2O_2 were added. In this case, the analysis shows a recovery percentage of 109 with a 5% of RSD. Since the recovery percentage is the sensor's response obtained from an amount of the analyte added to the matrix, compared to the sensor response for the true concentration of the pure analyte, the obtained results in both milk and cleaning liquid matrices demonstrate the versatility and applicability of our new ox-SWCNHs @CeO_2-based sensor for H_2O_2 detection in commercial products.

4. Conclusions

In this study, we designed a strategy to considerably improve the sensing ability of a moderate H_2O_2 sensor made of CeO_2. Such strategy is based on the integration of SWCNHs into the metal oxide through a simple but powerful synthetic protocol that allows the critical intimacy between the two phases. The functional hierarchical nano-catalyst was characterized by TGA, FTIR, Raman, TEM, EDX, AFM and electrochemistry. These analyses indicated the presence of CeO_2 covering uniformly the ox-SWCNHs and forming spherical particles with an average size of ~70 nm. The material is very homogenous, and the tight contact between the two phases is paramount to guarantee an efficient electronic communication, which ultimately leads to an outstanding performance toward the sensing of H_2O_2. The ox-SWCNHs@CeO_2 nanohybrid was used to assemble a working electrode and electro-catalyze the reduction of H_2O_2 with high sensitivity (160 ± 20 μA cm^{-2} mM^{-1}), two orders of magnitude bigger than the corresponding SWCNH-

free electrode, and up to level with the sensitivity reported for state-of-the art metal oxide-based sensors. The nanohybrid also displayed good stability (82% response after 2 weeks of continuous use) and reproducibility. The testing of the performance in commercial samples (commercial milk and cleaning liquid) confirmed that the as-modified electrode is capable of sustaining a remarkable selectivity toward hydrogen peroxide even in very complex matrix environments. The simplicity of assembly, the reduced cost, the outstanding performance and the flexibility of the newly developed nanohybrid, combined with future proper engineering of the electrode, project the material as a future reference sensor. From a wider perspective, the strategy employed could be extended, upon suitable setting of synthetic conditions, to other metal oxides and may lead to the establishment of a new class of commercial sensors for H_2O_2, able to compete with the enzyme-based sensors.

Acknowledgments

The authors acknowledge University of Trieste, ICCOM-CNR and INSTM Consortium, MIUR, Italy, through the project HI- PHUTURE (protocol 2010N3T9M4) and European Community through the project FP7-NMP-2012-SMALL-6 (project ID 310651) for financial support. The COST action CM1104 is also acknowledged. M.V.B. undertook this work with the support of the "ICTP TRIL Programme, Trieste, Italy"

Appendix A. Supplementary data

Supplementary data associated with this article can be found, in the online version, at http://dx.doi.org/10.1016/j.snb.2016.08.112.

References

[1] P. Tundo, V. Esposito, Green Chemical Reactions, Springer, Netherlands, 2008.
[2] M.S. Quintino, H. Winnischofer, K. Araki, H.E. Toma, L. Angnes, Cobalt oxide/tetraruthenated cobalt-porphyrin composite for hydrogen peroxide amperometric sensors, Analyst 130 (2005) 221–226.
[3] C. Reichardt, T. Welton, Solventsand Solvent Effects in Organic Chemistry, John Wiley & Sons, Nueva Jersey, Estados Unidos, 2011.
[4] J.R. Stone, S. Yang, Hydrogen peroxide: a signaling messenger, Antioxid. Redox Signal. 3–4 (2006) 243–270.
[5] European Comission, CosIngisthe European Commissiondatabaseforinformation on cosmetic substancesand ingredients contained in the Cosmetics Regulation Regulation (EC) No 1223/2009 ofthe European Parliament and of the Council; CosmeticsDirective 76/768/EEC (CosmeticsDirective), asamended; Inventory of Cosmetic Ingredients asamended by Decision 2006/257/EC establishing a common nomenclature of ingredients employed for labelling cosmetic products throughout the EUOpinions on cosmetic ingredients of the Scientific Committee for Consumer Safety. http://ec.europa.eu/growth/tools-databases/cosing/index.cfm, (accessed: April 2016).
[6] A.L. Hu, Y.H. Liu, H.H. Deng, G.L. Hong, A.L. Liu, X.H. Lin, X.H. Xia, W. Chen, Fluorescent hydrogen peroxide sensor based on cupric oxide nanoparticles and its application for glucose and L-lactate detection, Biosens. Bioelectron. 61 (2014) 374–378.
[7] Y.B. Tsaplev, Chemiluminescence determination of hydrogen peroxide, J. Anal. Chem. 67 (2012) 506–514.
[8] H.A. Khorami, J.F. Botero-Cadavid, P. Wild, N. Djilali, Spectroscopic detection of hydrogen peroxide with an optical fiber probe using chemically deposited Prussian blue, Electrochim. Acta 115 (2014) 416–424.
[9] Y. Hu, Z. Zhang, C. Yang, The determination of hydrogen peroxide generated from cigarette smoke with an ultrasensitive and highly selective chemiluminescence method, Anal. Chim. Acta 601 (2007) 95–100.
[10] S.K. Ujjain, A. Das, G. Srivastava, P. Ahuja, M. Roy, A. Arya, K. Bhargava, N. Sethy, S.K. Singh, R.K. Sharma, M. Das, Nanoceria based electrochemical sensor for hydrogen peroxide detection, Biointherphases 9 (2014) 031011.
[11] X. Chen, G. Wu, Z. Cai, M. Oyama, X. Chen, Advances in enzyme-free electrochemical sensors for hydrogen peroxide, glucose, and uric acid, Microchim. Acta. 181 (2014) 689–705.
[12] (a) G. Nie, X. Lu, J. Lei, L. Yang, X. Bian, Y. Tong, C. Wang, Sacrificial template-assisted fabrication of palladium hollow nanocubes and their application in electrochemical detection toward hydrogen peroxide, Electrochim. Acta 99 (2013) 145–151.
[13] A.J.S. Ahammad, Hydrogen peroxide biosensors based on horseradish peroxidase and hemoglobin, J. Biosens. Bioelectron. 9 (2013) 1–11.
[14] R. Breslow, Biomimetic chemistry and artificial enzymes: catalysis by design, Acc. Chem. Res. 28 (1995) 146–153.
[15] E. Shoji, M.S. Freund, Potentiometric sensors based on the inductive effect on the pK(a) of poly(aniline): a nonenzymatic glucose sensor, J. Am. Chem. Soc. 123 (2001) 3383–3384.
[16] W. Chen, S. Cai, Q.Q. Ren, W. Wen, Y.D. Zhao, Recent advances in electrochemical sensing for hydrogen peroxide: a review, Analyst 137 (2012) 49–58.
[17] N. Jia, B. Huang, L. Chen, L. Tan, S. Yao, A simple non-enzymatic hydrogen peroxide sensor using gold nanoparticles-graphene-chitosan modified electrode, Sens. Actuators B 195 (2014) 165–170.
[18] (a) H. Kivrak, O. Alal, D. Atbas, Efficient and rapid microwave-assisted route to synthesize Pt–MnOx hydrogen peroxide sensor, Electrochim. Acta 176 (2015) 497–503;
(b) J. Sophia, G. Muralidharan, Amperometric sensing of hydrogen peroxide using glassy carbon electrode modified with copper nanoparticles, Mater. Res. Bull. 15 (2015) 315–320.
[19] M. Melchionna, M. Bonchio, F. Paolucci, M. Prato, P. Fornasiero, Catalysis-material crosstalk at tailored nano-carbon interfaces, Top. Curr. Chem. 348 (2014) 139–180.
[20] (a) W. Tu, J. Lei, L. Ding, H. Ju, Sandwich nanohybrid of single-walled carbon nanohorns–TiO2–porphyrin for electrocatalysis and amperometric biosensing towards chloramphenicol, Chem. Commun. (2009) 4227–4229;
(b) N. Mutneja, K.R. Patil, S. Kurungot, Nitrogen-induced surface area and conductivity modulation of carbon nanohorn and its function as an efficient metal-free oxygen reduction electrocatalyst for anion-exchange membrane fuel cells, Small 11 (2015) 352–360;
(c) L. Deng, M. Zhu, Metal–nitrogen (Co-g-C3N4) doping of surface-modified single-walled carbon nanohorns for use as an oxygen reduction electrocatalyst, RSC Adv. 6 (2016) 25670–25677;
(d) S. Zhao, L. Wang, T. Wang, Q. Han, S. Xu, A high-performance hydrazine electrochemical sensor based on gold nanoparticles/single-walled carbon nanohorns composite film, Appl. Surf. Sci. 369 (2016) 36–42.
[21] S. Zhu, G. Xu, Single-walled carbon nanohorns and their applications, Nanoscale 2 (2010) 2538–2549.
[22] K. Murata, K. Kaneko, W.A. Steele, F. Kokai, K. Takahashi, D. Kasuya, K. Hibarahara, M. Yudasakaand, S. Iijima, Molecular potential structures of heat-treated single-wall carbon nanohorn assemblies, J. Phys. Chem. B 105 (2001) 10210–10216.
[23] (a) A. Hashimoto, H. Yorimitsu, K. Ajima, K. Suenaga, H. Isobe, J. Miyawaki, M. Yudasaka, S. Iijima, E. Nakamura, Selective deposition of a gadolinium(III) cluster in a hole opening of single-wall carbon nanohorn, PNAS 101 (2004) 8527–8530;
(b) E. Bekyarova, K. Murata, M. Yudasaka, D. Kasuya, S. Iijima, H. Tanaka, H. Kahoh, K. Kaneko, Single-wall nanostructured carbon for methane storage, J. Phys. Chem. B 107 (2003) 4681–4684.
[24] A.T. Lawal, Synthesis and utilization of carbon nanotubes for fabrication of electrochemical biosensor, Mater. Res. Bull. 73 (2013) 308–350.
[25] R.D. Costa, S. Feihl, A. Kahnt, S. Gambhir, D.L. Officer, G.G. Wallace, M.I. Lucio, M.A. Herrero, E. Vázquez, Z. Syrgiannis, M. Prato, D.M. Guldi, Carbon nanohorns as integrative materials for efficient dye-sensitized solar cells, Adv. Mater. 25 (2013) 6513–6518.
[26] F. Lodermeyer, R.D. Costa, R. Casillas, F.T.U. Kohler, P. Wasserscheid, M. Prato, D.M. Guldi, Carbon nanohorn-based electrolyte for dyesensitized solar cells, Energy Environ. Sci. 8 (2015) 241–246.
[27] R. Casillas, F. Lodermeyer, R.D. Costa, M. Prato, D.M. Guldi, Substituting TiCl4 – carbon nanohorn interfaces for dye-sensitized solar cells, Adv. Energy Mater. 4 (2014) 1301577–1301582.
[28] F. Lodermeyer, M. Prato, R.D. Costa, D.M. Guldi, Facile and quick preparation of carbon nanohorn-based counter electrodes for efficient dye-sensitized solar cells, Nanoscale 8 (2016) 7556–7591.
[29] S. Carli, L. Casarin, Z. Syrgiannis, R. Boaretto, E. Benazzi, S. Caramori, M. Prato, C.A. Bignozzi, Single walled carbon nanohorns as catalytic counter electrodes for Co(III)/(II) electron mediators in dye sensitized cell, ACS Appl. Mater. Interfaces 8 (23) (2016) 14604–14612.
[30] S. Zhu, L. Fan, X. Liu, L. Shi, H. Li, S. Han, G. Xu, Determination of concentrated hydrogen peroxide at single-walled carbon nanohorn paste electrode, Electrochem. Commun. 10 (2008) 695–698.
[31] L. Zhang, Y. Ni, X. Wang, G. Zhao, Direct electrocatalytic oxidation of nitric oxide and reduction of hydrogen peroxide based on α-Fe2O3 nanoparticles-chitosan composite, Talanta 82 (2010) 196–201.
[32] M. Montini, M. Melchionna, M. Monai, P. Fornasiero, Fundamentals and catalytic applications of CeO2-based materials, Chem. Rev. 116 (2016) 5987–6041.
[33] A. Trovarelli, P. Fornasiero, Catalysis by Ceria and Related Materials, Imperial College Press, United Kingdom, 2013.
[34] C. Sun, H. Li, L. Chen, Nanostructured ceria–based materials: synthesis, properties, and applications, Energy Environ. Sci. 5 (2012) 8475–8505.
[35] K. Zhou, Z. Yang, S. Yang, Highly reducible CeO2 nanotubes, Chem. Mater. 19 (2007) 1215–1217.
[36] B. Tang, L. Zhuo, J. Ge, G. Wang, Z. Shia, J. Niua, A surfactant-free route to single-crystalline CeO2 nanowires, Chem. Commun. (2005) 3565–3567.
[37] L. Wang, M. Deng, G. Ding, S. Chen, F. Xu, Manganese dioxide based ternary nanocomposite for catalytic reduction and nonenzymatic sensing of hydrogen peroxide, Electrochim. Acta 114 (2013) 416–423.

[38] H. Kivrak, O. Alal, D. Atbas, Constructing hierarchical porous titania microspheres from titania nanosheets with exposed (001) facets for dye-sensitized solar cells, Electrochim. Acta 175 (2015) 497–505.
[39] C.-Y. Lin, C.-T. Chang, Iron oxide nanorods array in electrochemical detection of H2O2, Sens. Actuators B 220 (2015) 695–704.
[40] A. Beltram, M. Melchionna, T. Montini, P. Fornasiero, Improved activity and stability of Pd@CeO2 core–shell catalysts hybridized with multi-walled carbon nanotubes in the water gas shift reaction, Catal. Today 253 (2015) 142–148.
[41] J.R. McBride, K.C. Hass, B.D. Poindexter, W.H. Werber, Raman and x-ray studies of Ce_{1-x} RE_x O_{2-y}, where RE = La, Pr, Nd, Eu, Gd, and Tb, J. Appl. Phys. 76 (1994) 2435–2441.
[42] X. Beaudoux, M. Virot, T. Chave, G. Durand, G. Leturcq, S.I. Nikitenko, Vitamin C boosts ceria-based catalyst recycling, Green Chem. 18 (2016) 3656–3668.
[43] M.S. Dresselhaus, A. Jorio, M. Hofmann, G. Dresselhaus, R. Saito, Perspectives on carbon nanotubes and graphene raman spectroscopy, Nano Lett. 3 (2010) 751–758.
[44] J.E. Spanier, R.D. Robinson, F. Zhang, S.-W. Chan, I.P. Herman, Size-dependent properties of CeO_{2-y} nanoparticles as studied by Raman scattering, Phys. Rev. B 64 (2001) 245407–245415.
[45] A.K. Yagati, T. Lee, J. Min, J.W. Choi, An enzymatic biosensor for hydrogen peroxide based on CeO2 nanostructure electrodeposited on ITO surface, Biosens. Bioelectron. 47 (2013) 385–390.
[46] F. D'Souza, Fullerenes, nanotubes, and carbon nanostructures, Electrochem. Soc. (2007).
[47] D. Joung, V. Singh, S. Park, A. Schlute, S. Seal, S.I. Khondaker, Anchoring ceria nanoparticles on reduced graphene oxide and their electronic transport properties, J. Phys. Chem. C 115 (2011) 24494–24500.
[48] J.H. Lee, H.G. Hong, Nonenzymatic electrochemical sensing of hydrogen peroxide based on a polyaniline-MnO2 nanofiber-modified glassy carbon electrode, J. App. Electrochem. 45 (2015) 1153–1162.
[49] J.C. Chen, W.C. Chen, Y.C. Tien, C.J. Shih, Effect of calcination temperature on the crystallite growth of cerium oxide nano-powders prepared by the co-precipitation process, J. Alloys Compd. 496 (2010) 364–369.
[50] A. Karakoti, S. Singh, J.M. Dowding, S. Sealac, W.T. Self, Redox-active radical scavenging nanomaterials, Chem. Soc. Rev. 39 (2010) 4422–4432.
[51] K. Sing, D. Everett, R. Haul, L. Moscou, R. Pierotti, J. Rouquerol, T. Siemieniewska, Reporting physisorption data for gas/solid systems with special reference to the determination of surface area and porosity, Pure Appl. Chem. 57 (1985) 603–619.
[52] U.S. Food and Drug Administration, Code of Federal Regulations, 21, 3, cite: 21CFR184.1366. Available on: http://www.accessdata.fda.gov/scripts/cdrh/cfdocs/cfcfr/CFRSearch.cfm?fr=184.1366, 2015 (accessed: 03.06.16).
[53] R.A.B. Silva, R.H.O. Montes, E.M. Richter, R.A.A. Munoz, Food Chem. 133 (2013) 200.

Biographies

Maurizio Prato graduated in Padova, Italy, where he was appointed Assistant Professor in 1983. Moved to Trieste as an Associate Professor in 1992, and then promoted to Full Professor in 2000. He spent a sabbatical terms at Yale University and at the University of California, Santa Barbara. He was Visiting Professor at Ecole Normale Supérieure Paris (2001), the University of Namur, Belgium (2010) and the University of Strasbourg (2014). He was the recipient of an ERC Advanced Research Grant, European Research Council, 2008 and became a Member of the National Academy of Sciences (Accademia Nazionale dei Lincei) in 2010. His research focuses on the application of organic chemistry to nanosciences for the preparation of new materials useful in the fields of energy and nanomedicine.

Paolo Fornasiero obtained the degree in Chemistry in 1992 and in 1997 the PhD at the University of Trieste (Italy). After a post-doctoral fellow at the University of Reading (U.K.), in 1998 he was appointed Assistant Professor and in 2006 associate professor in Inorganic Chemistry at the University of Trieste. He is Associate Researcher of the National Council of Research (CNR) and from 2008 he is the scientific responsible of the CNR Research Unit associated with the Institute of Chemistry of OrganoMetallic Compounds (ICCOM) of Florence. He has been visiting Professor at King Abdullah University of Science and Technology (KAUST) in Saudi Arabia. He is a member of the Italian Chemical Society, of the American Chemical Society, of the European Rare-Earth and Actinide Society – ERES, as well as of the INSTM Consortium. In 2015 he became Associate Editor of the journal ACS catalysis.